

Article

Study on Optical Positioning Using Experimental Visible Light Communication System

Nikoleta Vitsi ¹, Argyris N. Stassinakis ², Nikolaos A. Androutsos ¹, George D. Roumelas ¹,
George K. Varotsos ¹, Konstantinos Aidinis ³ and Hector E. Nistazakis ^{1,*}

¹ Section of Electronic Physics and Systems, Department of Physics, National and Kapodistrian University of Athens, 15784 Athens, Greece; sph1800245@uoa.gr (N.V.); nickandr@phys.uoa.gr (N.A.A.); groumelas@phys.uoa.gr (G.D.R.); georgevar@phys.uoa.gr (G.K.V.)

² Department of Computer Science and Biomedical Informatics, University of Thessaly, 35131 Lamia, Greece; a-stasinakis@phys.uoa.gr

³ Department of Electrical and Computer Engineering, Ajman University, Ajman P.O. Box 346, United Arab Emirates; k.aidinis@ajman.ac.ae

* Correspondence: enistaz@phys.uoa.gr; Tel.: +30-2107276710

Abstract: Visible light positioning systems (VLP) have attracted significant commercial and research interest because of the many advantages they possess over other applications such as radio frequency (RF) positioning systems. In this work, an experimental configuration of an indoor VLP system based on the well-known Lambertian light emission, is investigated. The corresponding results are also presented, and show that the system retains high enough accuracy to be operational, even in cases of low transmitted power and high background noise.

Keywords: optical positioning system; visible light communications; indoor VLP; Lambertian



Citation: Vitsi, N.; Stassinakis, A.N.; Androutsos, N.A.; Roumelas, G.D.; Varotsos, G.K.; Aidinis, K.; Nistazakis, H.E. Study on Optical Positioning Using Experimental Visible Light Communication System. *Computation* **2023**, *11*, 161. <https://doi.org/10.3390/computation11080161>

Academic Editors: Yudong Zhang and Francesco Cauteruccio

Received: 27 June 2023

Revised: 10 August 2023

Accepted: 12 August 2023

Published: 14 August 2023



Copyright: © 2023 by the authors. Licensee MDPI, Basel, Switzerland. This article is an open access article distributed under the terms and conditions of the Creative Commons Attribution (CC BY) license (<https://creativecommons.org/licenses/by/4.0/>).

1. Introduction

During the past years, free space optical (FSO) communications and, more precisely, visible light communication (VLC) systems have attracted considerable scientific and commercial interest because of the many advantages these systems offer over other Radio Frequency (RF) applications, and also because of the prospects of even greater technological improvements. The most significant of these advantages are the transmission at very high data rates, the low installation and operation costs, the high security level, operation within the unlicensed spectrum of visible light, and the robustness to electromagnetic interference, etc. [1,2]. Many references in the open technical literature demonstrate that the visible light communication systems utilizing either light-emitting diodes (LEDs) or lasers could be quite a promising alternative for present-day and even future high-capacity wireless networks [3–6].

Over the past years, there has been a remarkable increase in the activities of indoor positioning systems (IPS) given the growing development in emerging fields such as the Internet of Things (IoT) and wireless sensor networks [7]; moreover, location-based services have become an important part of our daily life [8]. Traditional indoor positioning systems, which are based on the radio frequencies, are not so accurate because of fading due to multipathing and signal penetration, while systems operating via ultrasound and infrared radiation need more resources [7]. In contrast, a technique that has become dominant and covers a wide field of applications is optical positioning [9]. The operation of IPS based on light-emitting diodes (LEDs) has attracted more significant academic and industrial interest due to the general advantages of VLC systems [10], but also because of the high positioning accuracy [7]. Indeed, similar to the Global Positioning System (GPS), which is widely used in outdoor environments, visible light positioning (VLP) can provide the navigation information to find the target indoor destinations. It can therefore be utilized

inside large buildings such as for asset tracking in hospitals or universities, for indoor positioning applications for blind people, as well as to provide location-aware services, such as antique information in museums or item prices in shopping malls [11,12].

In basic terms, a typical indoor VLP system consists of three or more different LEDs at the transmitter side, the VLC transmission link, and a photodetector (equipped with a photodiode) or a camera at the receiver side. In order to accurately determine the position of the receiver, apart from decoding the arriving encoded signal, different data may need to be obtained, such as the received signal strength, the noise level, the time of arrival, or the angle of arrival. The type of information needed is based on the particular positioning algorithm employed. The major positioning techniques to perform such a location estimation, include the received signal strength (RSS), time of arrival (TOA), time difference of arrival (TDOA), and AOA (angle of arrival) [13]. Among them, RSS is the most widely investigated mainly due to its high positioning accuracy and low cost [8]. Meanwhile, positioning 3D static targets and 2D fast moving targets are emerging research directions [14–17]. In more detail, the indoor positioning methods based on VLC are mainly distinguished as proximity, triangulation, and image positioning [7]. The proximity method provides only proximity location information on how close the optical receiver is to an optical transmitter and it is the simplest location sensing method but with an accuracy as good as the resolution of the grid [18,19]. Through the triangulation method, the target's position is evaluated by distance measurements from at least three reference locations [20–23] utilizing RSS, TOA, and TDOA techniques. Triangulation determines the absolute position by using the geometric properties of triangles. Here, we should clarify that there are two derivations of triangulation: lateration and angulation. Lateration techniques, which involve the TOA, the time difference TDOA, and RSS, estimate the position based on the measured distances from the mobile device to multiple LED transmitters. In this context, trilateration refers to the use of three LEDs. The angulation technique by means of AOA relies on the measured angles relative to multiple LEDs to determine the position of the mobile receiver terminal [19]. Note that perfect synchronization between the transmitter and receiver terminals is required for TOA and TDOA, while in order to accurately determine the distances through RSS, the optical receiver needs to receive signals from multiple transmitters with no interference [24,25]. Finally, the image positioning method evaluates the position of the receiver based on the coordinates of LEDs in the real world and in the image, which makes this method complex and cumbersome, as reflected in [7].

In this work, by taking into account the benefits of VLC systems, we propose an optical indoor positioning system using three white LEDs in the ceiling of a room; then, we present the theoretical analysis of the Lambertian considered model and the analysis along with evaluation of the corresponding experimental results of our setup.

Thus, the remainder of this work can be organized as follows: in Section 2, the theoretical background of the Lambertian model is analyzed, while in Section 3 the experimental setup and configuration is presented. Next, in Section 4, the corresponding experimental results are presented, and finally, the concluding remarks are shown in Section 5.

2. Theoretical Analysis of the Model

Considering the properties and the state of the system, two models are commonly used for the mathematical description of the channel, the Lambertian model [23–26] and the exponential model [22,27]. When the channel is characterized by an unhindered connection path between transmitter and receiver (the line-of-sight case), the Lambertian model is used, while the exponential model is employed when lenses are installed in front of the LEDs.

The radiation pattern of an LED diode is best described by the Lambertian model, which is generally used for the estimation of irradiance of every light source. In the case of

an LED lamp, the mathematical equation that estimates the optical power in a certain point has the following form [28–32]:

$$P_r = P_t \frac{(m+1)A}{2\pi D^2} \cos^m(\varphi) T_s(\varphi) g(\psi) \cos(\psi) \quad (1)$$

$$m = -\frac{\ln(2)}{\ln(\cos(\Phi_{1/2}))} \quad (2)$$

where P_r and P_t are the optical power received and transmitted respectively, A is the physical area of the detector, D is the distance between the transmitter and the receiver, T_s is the gain of the optical filter, g is the gain of the concentrator, Ψ_c is the width of the field of view of the receiver, ψ is the angle of incidence, and φ is the angle of irradiance.

The most commonly used positioning algorithm is the trilateration algorithm, which is based on estimating the geometric locus of the possible locations of the receiver for each reference point-LED and finding the intersection point of the curves. Taking the distance from the LED into account, the possible position of the receiver can be located on the circle in a two-dimensional plane or the sphere in a three-dimensional space, with the radius equal to the distance. For a positioning system deploying multiple LEDs, each LED creates its own circle or sphere, which corresponds to the possible positions of the receiver, calculated by the specific LED. In order to estimate the position of the receiver, the intersection point of the circles or spheres has to be calculated [32–37].

The estimation of the distance from each LED is usually achieved by measuring the received signal strength (RSS) or the time difference of arrival (TDOA). Especially when using a photodiode as the receiver, the received optical power can be easily estimated by the output voltage obtained from the photodiode datasheet. The distance from the transmitter is calculated by the selected channel model of the system. In contrast, the second technique, the TDOA, takes advantage of the phase difference of the received optical signals for the calculation of the distance. Supposing that the LEDs are perfectly synchronized to each other, the phase difference indicates the propagation time of the optical pulse, which in turn enables the estimation of the distance between the LED and the photoreceiver [32,36]. However, the latter technique is applicable only when a photodiode is employed at the receiving end.

Having successfully acquired the distance values from each LED transmitter, by applying the appropriate method, the required mathematical equations can be extracted. Considering the case of locating the receiver on a flat surface, the equations derived for the estimation of the coordinates (x, y) of the target have the following form [34,35,37]:

$$(x - x_i)^2 + (y - y_i)^2 = d_i^2 \quad (3)$$

where (x_i, y_i) are the coordinates of the center of the circle that is equivalent to the location of the i -th LED that transmitted the pulse and d_i the respective distance. The coordinates of the receiver are evaluated by solving the derived system of equations.

3. Experimental Setup and Process

3.1. Experimental Radiation Pattern of LEDs

The aim of the first part of the experimental procedure is to extract an experimental radiation pattern for the cold white LEDs. More specifically, a 5 Watt star LED will be used with half-angle radiation 60 degrees. In contrast, the receiver will consist of the photodiode BPW21. In order to drive the LED and the photodiode respectively, the following circuits, depicted in Figure 1 for the transmitter and the receiver, were deployed:

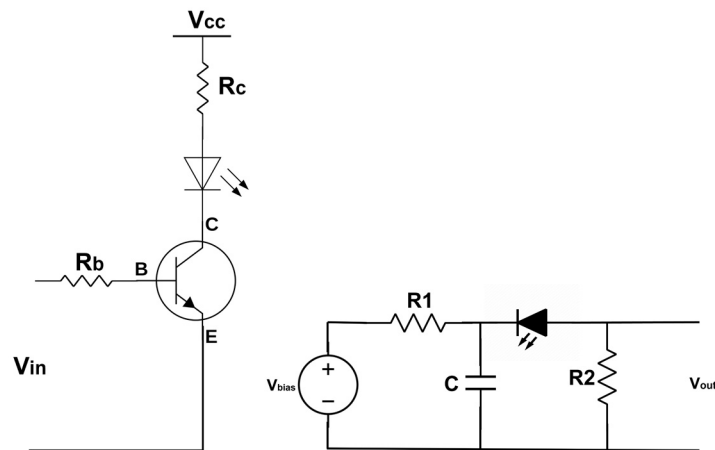


Figure 1. Optical transmitter and receiver. All the parameter values appear in Table 1.

Table 1. Technical specifications of optical transmitter and receiver.

Transmitter		Receiver	
Vcc	24 V	Vc	5 V
Rc	50 Ω/100 Ω/150 Ω/200 Ω	R1	1 kΩ
Rb	1 kΩ	R2	390 kΩ
BJT	BD139	C	47 nF
Vin	5 V		

The technical characteristics of the circuits of Figure 1 are presented in the following table:

The values of Table 1 for R1, R2, and C were selected to deploy a receiver with high sensitivity and at the same time to avoid any voltage saturation, after a wide range of values were tested in the lab. The transmitter and the receiver will be placed on the same plane with the LED having the ability to slide on the x axis and photodiode on the y axis. Furthermore, the photodiode’s plane is always parallel to the LED plane so the orientation angle of the photodiode does not affect the system [38]. The schematic of the experimental setup is presented in Figure 2:

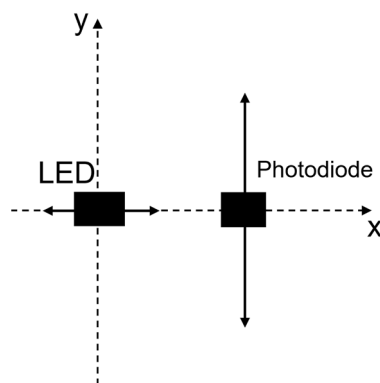


Figure 2. Experimental setup schematic.

Using the above setup, the voltage at the output of the receiver circuit will be measured for various distances between the transmitter and the receiver. The LED will transmit optical power, which will be received by photodiode, and the generated output signal will be a number of pulses. To generate these pulses, we will build a code (via Arduino) where the duration of each pulse of LED (duration that LED illuminates), and the duration that

LED is off will have fixed values. For the photodiode, in order to take measurements, we will build a suitable code (via Arduino) that will receive the transmitted output signal. The purpose of using pulses is to measure the background noise when the LED is off and abstract its mean value from the mean value of the pulse so that the impact of optical noise is negligible. For higher accuracy during the experimental procedure, the background optical noise was low and stable. Using the experimental measurements and Equation (1), an experimental model will be extracted that will have the following form:

$$V_r = \frac{C}{x^2 + y^2} \left(\frac{x^2}{x^2 + y^2} \right) \tag{4}$$

where V_r is the voltage at the output of the receiver, which has a linear relationship with optical power, and C is a constant that includes all technical characteristics that are fixed for a specific diode. The value of C will be calculated after fitting the experimental results with the theoretical expected results of the Lambertian model.

3.2. Positioning

For the optical positioning system, an experimental setup that will consist of three cold white LEDs will be constructed. For simplicity in trilateration calculations, the LED transmitters will be placed on the x and y axis and the area where the receiver can be tracked will be between the LEDs. This setup is depicted in Figure 3 below:

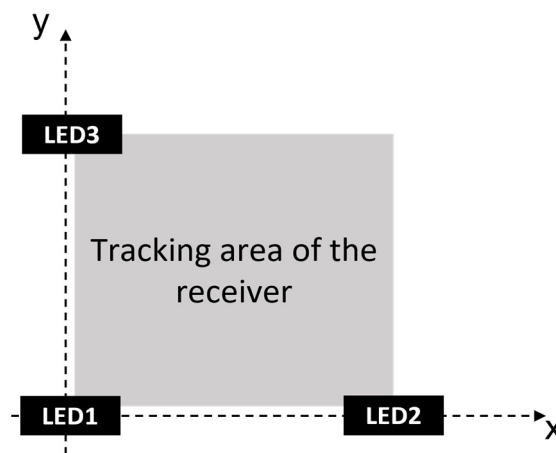


Figure 3. Positioning experimental setup.

In order to calculate the position of the photodiode, several pulses will be emitted from each photodiode in certain time slots. More precisely, a time slot will consist of a pilot pulse that will be emitted from all LEDs simultaneously with a fixed pulse width. The time at the beginning of this pulse will be the $t_0 = 0$ s of the time slot so that the receiver’s system can synchronize with the transmitter. Then, each LED will emit a pulse at a certain time. The pulse series that the photodiode will receive in each time slot is presented in Figure 4:

These pulses will create a voltage signal at the output of the photodiode circuit that will be collected using an Arduino system. The voltage amplitude of each pulse at the receiver will be used to calculate the radius of the circles that are formed on the plane of the receiver between the coordinates of each LED and the spot of the photodiode using the following equation:

$$r = \sqrt{\sqrt{\frac{h^2 C}{V_r}} - h^2} \tag{5}$$

where h is the distance between the LED and the plane of receiver.

The radius values that are calculated will be used in the trilateration method described above in order to estimate the coordinates of the receiver’s photodiode. Due to the high

complexity of the method, the pulses at the receiver will be transmitted in the Python environment where the process will be implemented in real time.

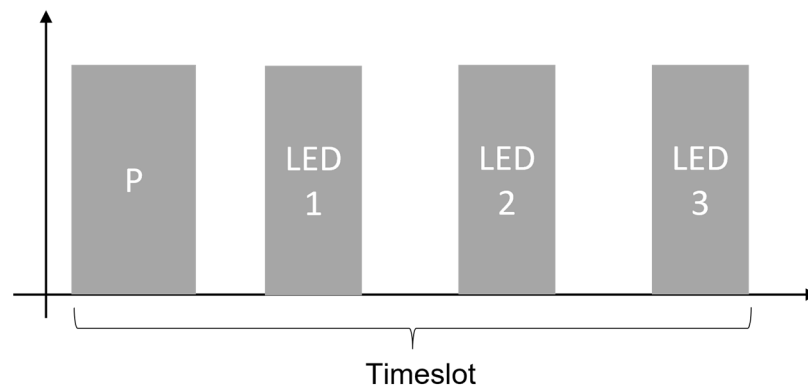


Figure 4. Pulses of positioning system.

4. Results and Discussion

In this section, the results of the experimental procedure that was described above will be presented. Although the same type of LED was used for each transmitter, the radiation pattern was examined for every LED separately to decrease the error in the real environment. This procedure will help to investigate the limits of the system in a real environment with higher accuracy. In order to extract the experimental optical power pattern of each LED, the voltage at the output of the receiver was measured for various distances between the receiver and the transmitter. More precisely, the values of distance x were $x = [0.10, 0.15, 0.20, 0.25, 0.30, 0.35, 0.40, 0.45]$ m and the values of distance y were $y = [0, 0.1, 0.2, 0.3]$ m. Furthermore, the procedure was repeated for various values of LED transmitted power, P_L , in order to experimentally calculate the dependence between the optical power transmitted and the voltage at the output of the receiver. The experimental results after fitting procedure using linear regression are presented in Figure 5.

In Figure 5, it can be observed that the fitting is more accurate as the distance increases. That was expected as the slot of the curve decreases. In addition, in case of $y = 0$, for x lower than 0.15 m, the receiver is saturated as the voltage source that is used is 5 V, so every higher value is expected to be saturated to 5 V. This fact is expected to have a negligible impact on the performance of the system as it will be used for much higher distance values. According to these results, the constant c that was extracted after applying the linear regression is presented for each LED and P_L in Table 2.

Table 2. Constant C values.

	PL = 1.5 W			PL = 0.8 W		
	y = 0 m	y = 0.1 m	y = 0.15 m	y = 0 m	y = 0.1 m	y = 0.15 m
LED1	0.175	0.172	0.171	0.095	0.093	0.095
LED2	0.17	0.175	0.18	0.091	0.096	0.094
LED3	1.165	0.172	0.175	0.095	0.092	0.097

For the positioning procedure, four cases were examined for different values of height, i.e., $h_1 = 0.22$ m and $h_2 = 0.28$ m, LED power transmitted, i.e., $PL1 = 1.5$ W and $PL2 = 0.8$ W, and background noise, i.e., low noise with room lights turned off and high noise with room lights turned on. The height of the LED transmitters was set to two different values, $h_1 = 0.22$ m and $h_2 = 0.26$ m, with the maximum range in the x or y axis for accurate enough results being around 0.5 m. In the case of higher values of h , the range of the system is expected to be decreased. In all cases, the receiver’s photodiode was placed in nine fixed spots with the coordinates being $s = [0.05, 0.05], [0.15, 0.05], [0.25, 0.05], [0.05, 0.15], [0.15, 0.15], [0.25, 0.15], [0.05, 0.25], [0.15, 0.25], [0.25, 0.25]$ m. More specifically, the cases are presented in Table 3.

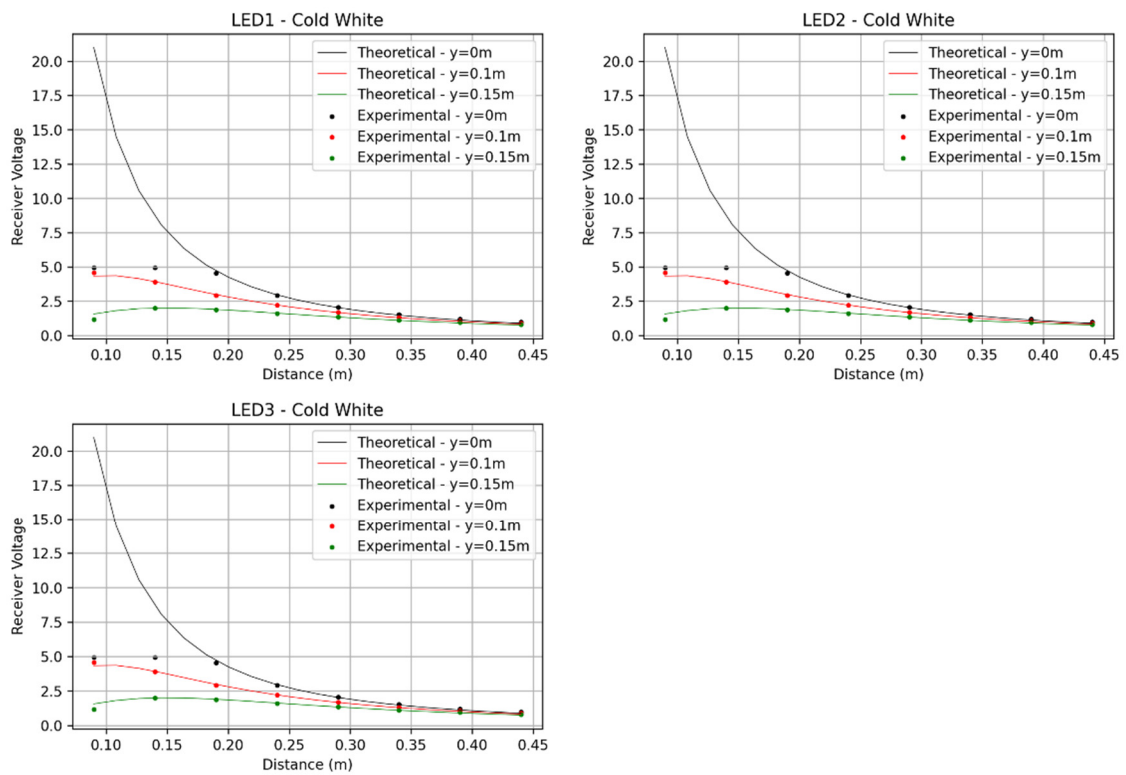


Figure 5. Regression fitting results.

Table 3. Case studies details.

	Height	PL	Noise
Case 1	0.22 m	1.5 W	Low
Case 2	0.26 m	1.5 W	Low
Case 3	0.26 m	0.8 W	Low
Case 4	0.26 m	0.8 W	High

The signals received for every case are presented in Figure 6.

Then, after processing the signals above, the distance between the receiver and the center of the LED on the receiver’s plane was calculated. Using these distances and the trilateration method that was described above, the coordinates of the receiver were extracted. The results for every case are presented in Figures 7 and 8.

From the outcomes appear in Figures 7 and 8 it can be seen that for the same value of power transmitted, the system presents higher accuracy when the receiver is closer to the LED transmitter while the accuracy decreases when the photodiode reaches the limit of the area.

By observing Figures 9 and 10, the accuracy of the system remains high, even for half transmitted power and even for high background noise. Such results are very important as the system is operational for a wide range of transmitted power and is not affected by the background noise, so it can be used as a primary system in a room for lighting and positioning or as a secondary system only for positioning without being affected by other light sources in the room.

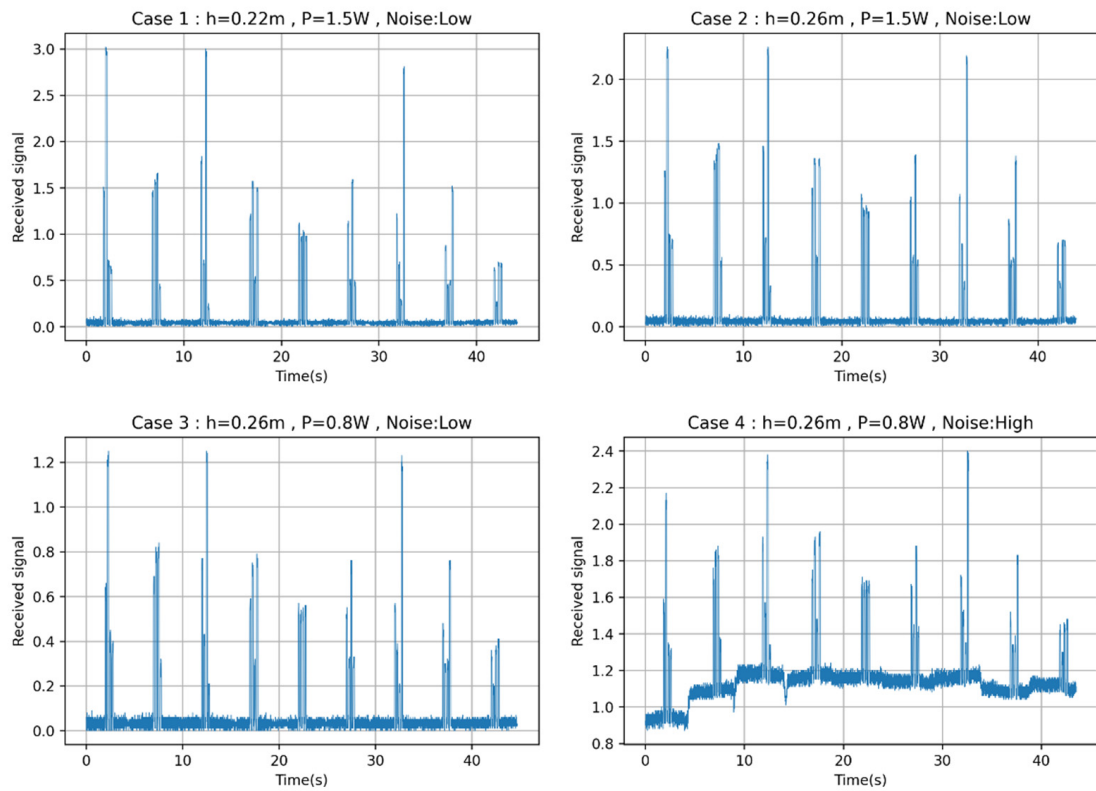


Figure 6. Signal received in each case.

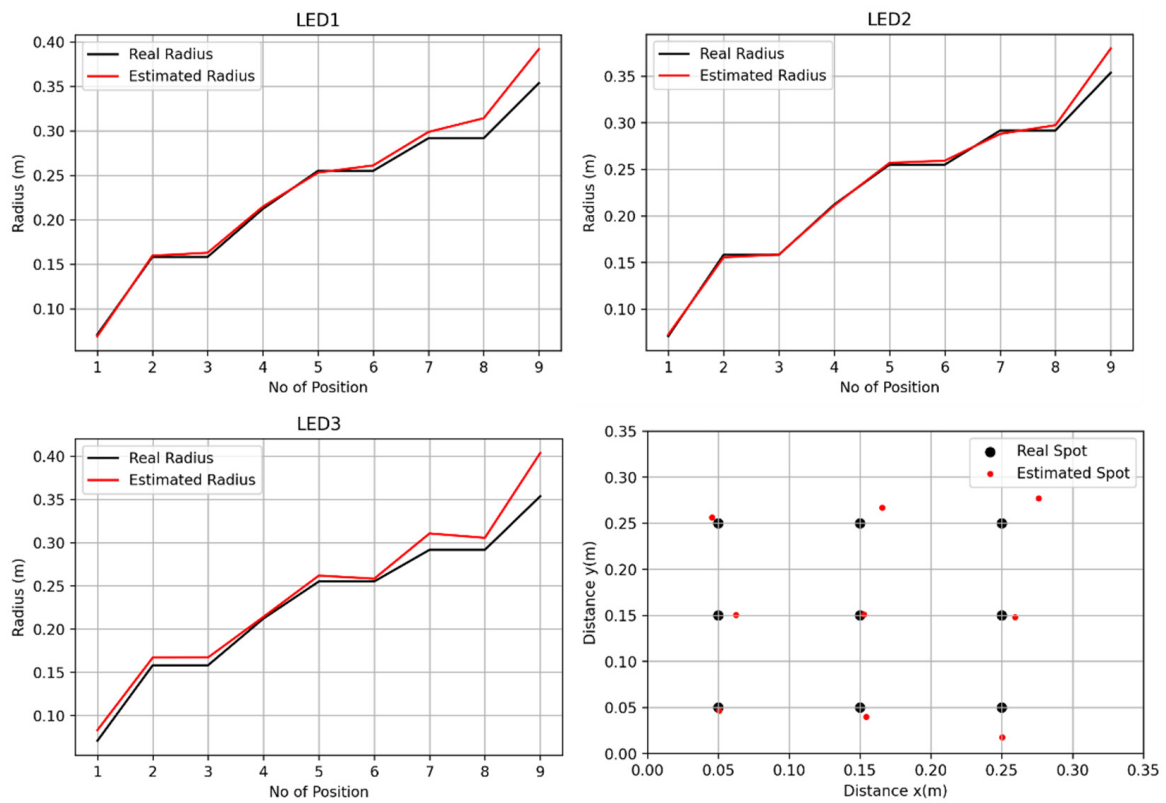


Figure 7. Case 1 results.

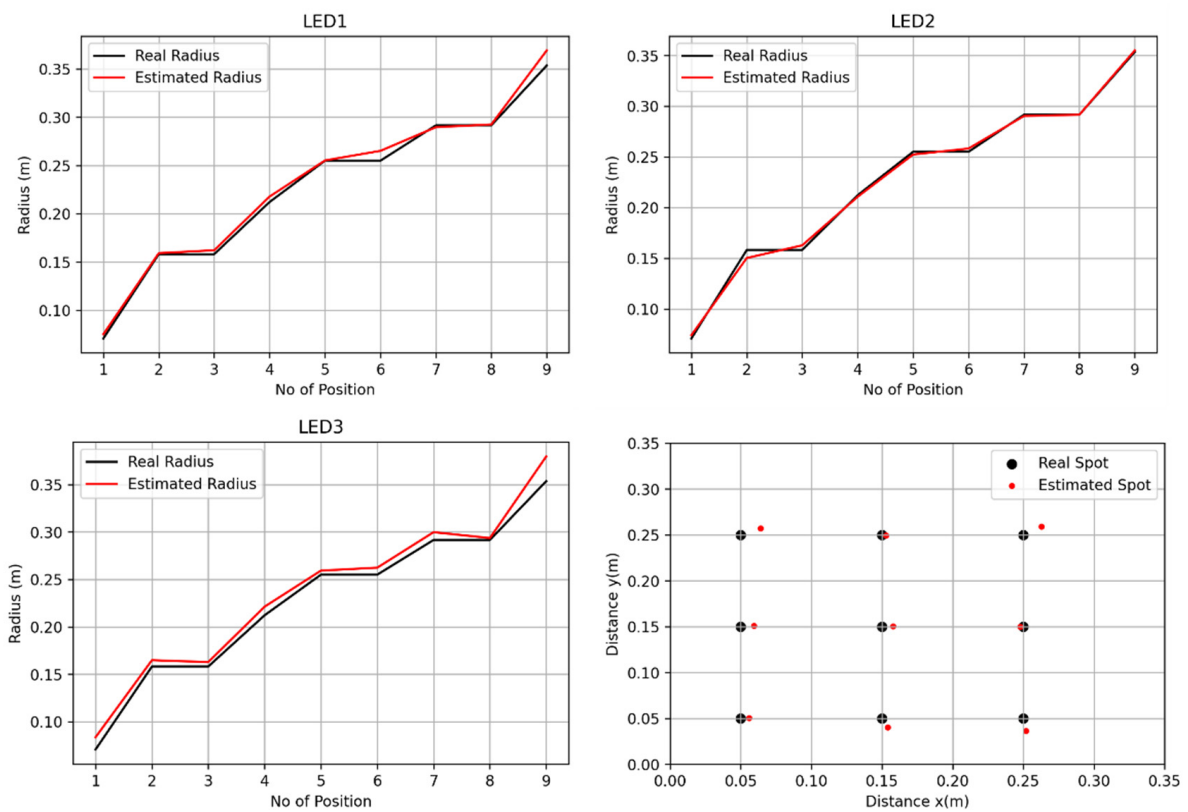


Figure 8. Case 2 results.

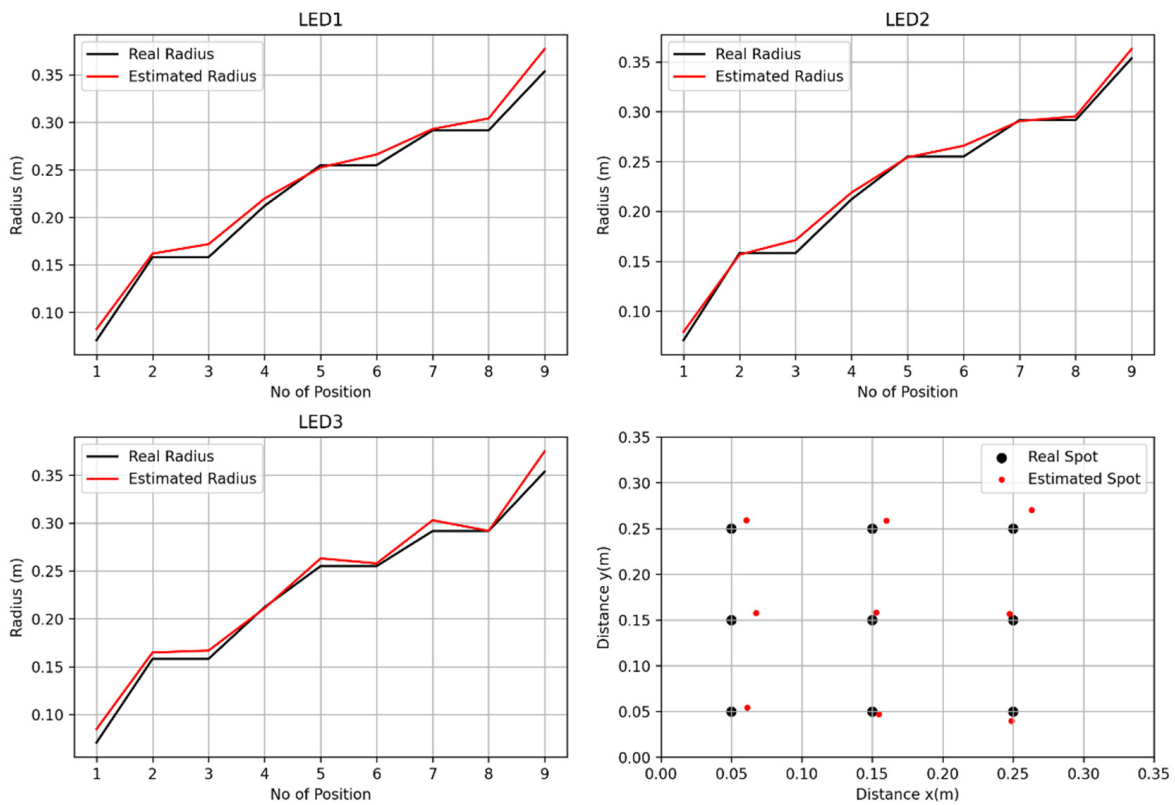


Figure 9. Case 3 results.

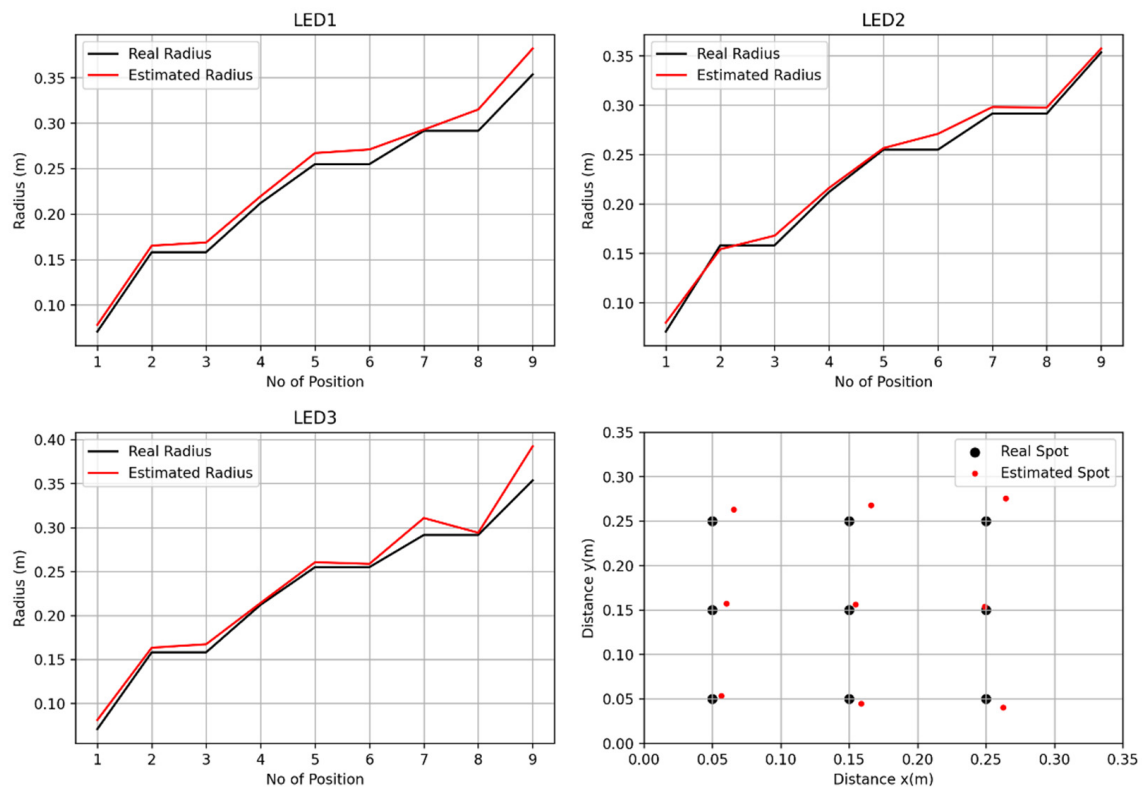


Figure 10. Case 4 results.

In order to evaluate the accuracy of the system, the root mean squared error (RMSE) and the mean absolute error (MAE) were calculated for the radius prediction of every case and for the coordinated of every spot in every case. The corresponding results are presented in Table 4.

Table 4. Case studies details.

	Case 1	Case 2	Case 3	Case 4
RMSE LED 1	0.0155	0.0062	0.1177	0.0151
RMSE LED 2	0.0094	0.0036	0.0075	0.0079
RMSE LED 3	0.0193	0.0112	0.0103	0.0154
RMSE x axis	0.0111	0.0079	0.0096	0.0112
RMSE y axis	0.0153	0.0068	0.0097	0.0123
MAE LED1	0.0083	0.0044	0.0092	0.0127
MAE LED2	0.0032	0.0001	0.0054	0.0059
MAE LED 3	0.0143	0.0091	0.0079	0.0107
MAE x axis	0.0072	0.0061	0.0072	0.0097
MAE y axis	0.0002	0.0007	0.0056	0.0068

The very low values of the RMSE indicate a very small deviation from the residual ground truth. Thus, the accuracy of the model is very high for all of the four cases that were studied. When comparing these results to the results of other works concerning optical wireless positioning systems [7,8], the errors and the accuracy are generally similar or even better. The differences in the results between all these works are due to differences in the experimental setup that is used each time, i.e., the use of an optical camera instead of a photodiode. Therefore, a quantitative comparison between the results of each method is not significant.

According to the above results, this system is operational in the case that there are no obstacles in the area. In the case that an obstacle blocks the line of sight between the receiver and the transmitter, the accuracy of the system will be significantly decreased. In

addition, the presence of multiple light sources with high power may cause saturation at the receiver.

5. Conclusions

In this work, a visible light positioning system with three cold white LEDs was experimentally investigated. A theoretical study of the Lambertian model was carried out as it is a very significant model for such applications. Then, an experimental configuration was developed and analyzed based on this model, and by considering the experimental measurements, the corresponding experimental results were presented, showing the fairly high accuracy of the indoor optical positioning system. The results show that the system is very accurate and the impact of the optical power transmitted and background noise is negligible as long as the total power is higher than the optical threshold and it is not saturated. Finally, VLP systems can be easily implemented provided that there is a VLC system already in use and an appropriate photodiode is installed on the device requiring positioning. The inexpensive and simple implementation of these systems has raised interest and the need for further study to improve their performance. To follow on from the current work, it is very important to scale up the employed setup in order to study cases that approximate real-life scenarios and investigate the effect of various combinations and orientations of LEDs.

Author Contributions: Conceptualization, A.N.S. and N.V.; methodology, A.N.S.; software, A.N.S. and N.A.A.; validation, G.D.R., G.K.V., and K.A.; formal analysis, N.V.; investigation, G.D.R., A.N.S., and H.E.N.; resources, N.A.A.; data curation, N.V.; writing—original draft preparation, G.D.R., N.A.A., and G.K.V.; writing—review and editing, H.E.N. and K.A.; visualization, N.V.; supervision, H.E.N. All authors have read and agreed to the published version of the manuscript.

Funding: This research received no external funding.

Conflicts of Interest: The authors declare no conflict of interest.

References

1. Farid, A.A.; Hranilovic, S. Outage Capacity Optimization for Free-Space Optical Links with Pointing Errors. *J. Light. Technol.* **2007**, *25*, 1702–1710. [[CrossRef](#)]
2. AlQuwaiee, H.; Ansari, I.S.; Alouini, M.-S. On the Performance of Free-Space Optical Communication Systems Over Double Generalized Gamma Channel. *IEEE J. Sel. Areas Commun.* **2015**, *33*, 1829–1840. [[CrossRef](#)]
3. Jayasudha, S.; Bakkiyalakshmi, N.; Manju, M.; Sivabarani, R.; Subasridevi, M. Visible Light Communications For 5g Wireless Networking Technology. *Adv. Nat. Appl. Sci.* **2016**, *10*, 390–395.
4. Manousou, D.K.; Stassinakis, A.N.; Syskakis, E.; Nistazakis, H.E.; Gardelis, S.; Tombras, G.S. Experimental Implementation and Theoretical Investigation of a Vanadium Dioxide Optical Filter for Bit Error Rate Enhancement of Enhanced Space Shift Keying Visible Light Communication Systems. *Computation* **2019**, *7*, 30. [[CrossRef](#)]
5. Manousou, D.K.; Stassinakis, A.N.; Syskakis, E.; Nistazakis, H.E.; Tombras, G.S.; Volos, C.K.; Tsigopoulos, A.D. Estimation of the Influence of Vanadium Dioxide Optical Filters at the Performance of Visible Light Communication Systems. In Proceedings of the 2018 7th International Conference on Modern Circuits and Systems Technologies (MOCASST), Thessaloniki, Greece, 7–9 May 2018; IEEE: New York, NY, USA, 2018; pp. 1–4. [[CrossRef](#)]
6. Menounou, S.; Stassinakis, A.N.; Nistazakis, H.E.; Tombras, G.S.; Sandalidis, H.G. Coverage Area Estimation for High Performance ESK Visible Light Communication Systems. In Proceedings of the 2017 Panhellenic Conference on Electronics and Telecommunications (PACET), Xanthi, Greece, 17–19 November 2017; IEEE: New York, NY, USA, 2017; pp. 1–4. [[CrossRef](#)]
7. Lin, B.; Ghassemlooy, Z.; Lin, C.; Tang, X.; Li, Y.; Zhang, S. An Indoor Visible Light Positioning System Based on Optical Camera Communications. *IEEE Photonics Technol. Lett.* **2017**, *29*, 579–582. [[CrossRef](#)]
8. Chen, Y.; Zheng, H.; Liu, H.; Han, Z.; Ren, Z. Indoor High Precision Three-Dimensional Positioning System Based on Visible Light Communication Using Improved Hybrid Bat Algorithm. *IEEE Photonics J.* **2020**, *12*, 6802513. [[CrossRef](#)]
9. Mautz, R.; Tilch, S. Survey of Optical Indoor Positioning Systems. In Proceedings of the 2011 International Conference on Indoor Positioning and Indoor Navigation, Guimaraes, Portugal, 21–23 September 2011.
10. Elgala, H.; Mesleh, R.; Haas, H. Indoor Optical Wireless Communication: Potential and State-of-the-Art. *IEEE Commun. Mag.* **2011**, *49*, 56–62. [[CrossRef](#)]

11. Wu, Y.-C.; Hsu, K.-L.; Liu, Y.; Hong, C.-Y.; Chow, C.-W.; Yeh, C.-H.; Liao, X.-L.; Lin, K.-H.; Chen, Y.-Y. Using Linear Interpolation to Reduce the Training Samples for Regression Based Visible Light Positioning System. *IEEE Photonics J.* **2020**, *12*, 7901305. [[CrossRef](#)]
12. Beguni, C.; Done, A.; Căilean, A.-M.; Avătămăniței, S.-A.; Zadobrischi, E. Experimental Demonstration of a Visible Light Communications System Based on Binary Frequency-Shift Keying Modulation: A New Step toward Improved Noise Resilience. *Sensors* **2023**, *23*, 5001. [[CrossRef](#)]
13. Keskin, M.F.; Gezici, S.; Arıkan, O. Direct and Two-Step Positioning in Visible Light Systems. *IEEE Trans. Commun.* **2018**, *66*, 239–254. [[CrossRef](#)]
14. Lin, P.; Hu, X.; Ruan, Y.; Li, H.; Fang, J.; Zhong, Y.; Zheng, H.; Fang, J.; Jiang, Z.L.; Chen, Z. Real-Time Visible Light Positioning Supporting Fast Moving Speed. *Opt. Express* **2020**, *28*, 14503. [[CrossRef](#)] [[PubMed](#)]
15. Fang, J.; Yang, Z.; Long, S.; Wu, Z.; Zhao, X.; Liang, F.; Jiang, Z.L.; Chen, Z. High-Speed Indoor Navigation System Based on Visible Light and Mobile Phone. *IEEE Photonics J.* **2017**, *9*, 8200711. [[CrossRef](#)]
16. Guan, W.; Chen, S.; Wen, S.; Tan, Z.; Song, H.; Hou, W. High-Accuracy Robot Indoor Localization Scheme Based on Robot Operating System Using Visible Light Positioning. *IEEE Photonics J.* **2020**, *12*, 7901716. [[CrossRef](#)]
17. Guan, W.; Zhang, X.; Wu, Y.; Xie, Z.; Li, J.; Zheng, J. High Precision Indoor Visible Light Positioning Algorithm Based on Double LEDs Using CMOS Image Sensor. *Appl. Sci.* **2019**, *9*, 1238. [[CrossRef](#)]
18. Lee, Y.U.; Baang, S.; Park, J.; Zhou, Z.; Kavehrad, M. Hybrid Positioning with Lighting LEDs and Zigbee Multihop Wireless Network. In Proceedings of the Broadband Access Communication Technologies VI, San Francisco, CA, USA, 24 January 2012; p. 82820L. [[CrossRef](#)]
19. Do, T.-H.; Yoo, M. An In-Depth Survey of Visible Light Communication Based Positioning Systems. *Sensors* **2016**, *16*, 678. [[CrossRef](#)] [[PubMed](#)]
20. Yang, S.-H.; Kim, H.-S.; Son, Y.-H.; Han, S.-K. Three-Dimensional Visible Light Indoor Localization Using AOA and RSS With Multiple Optical Receivers. *J. Light. Technol.* **2014**, *32*, 2480–2485. [[CrossRef](#)]
21. Kim, H.-S.; Kim, D.-R.; Yang, S.-H.; Son, Y.-H.; Han, S.-K. An Indoor Visible Light Communication Positioning System Using a RF Carrier Allocation Technique. *J. Light. Technol.* **2013**, *31*, 134–144. [[CrossRef](#)]
22. Wang, T.Q.; Sekercioglu, Y.A.; Neild, A.; Armstrong, J. Position Accuracy of Time-of-Arrival Based Ranging Using Visible Light With Application in Indoor Localization Systems. *J. Light. Technol.* **2013**, *31*, 3302–3308. [[CrossRef](#)]
23. Jung, S.-Y.; Hann, S.; Park, C.-S. TDOA-Based Optical Wireless Indoor Localization Using LED Ceiling Lamps. *IEEE Trans. Consum. Electron.* **2011**, *57*, 1592–1597. [[CrossRef](#)]
24. Ghassemlooy, Z.; Popoola, W.; Rajbhandari, S. *Optical Wireless Communications System and Channel Modelling with 354 MATLAB*; Taylor & Francis Group: Abingdon, UK; CRC Press: Boca Raton, FL, USA, 2013.
25. Matta, G.; Bahl, R.; Agarwal, M. Capacity Analysis of Indoor Visible Light Communication Systems. In Proceedings of the 2019 Global LIFI Congress (GLC), Paris, France, 12–13 June 2019; IEEE: New York, NY, USA, 2019; pp. 1–4. [[CrossRef](#)]
26. Tronghop, D.; Hwang, J.; Jung, S.; Shin, Y.; Yoo, M. Modeling and Analysis of the Wireless Channel Formed by LED Angle in Visible Light Communication. In Proceedings of the International Conference on Information Network 2012, Bali, Indonesia, 1–3 February 2012; IEEE: New York, NY, USA, 2012; pp. 354–357. [[CrossRef](#)]
27. Yang, S.-H.; Jung, E.-M.; Han, S.-K. Indoor Location Estimation Based on LED Visible Light Communication Using Multiple Optical Receivers. *IEEE Commun. Lett.* **2013**, *17*, 1834–1837. [[CrossRef](#)]
28. Bhalerao, M.V.; Sumathi, M.; Sonavane, S.S. Line of Sight Model for Visible Light Communication Using Lambertian Radiation Pattern of LED. *Int. J. Commun. Syst.* **2017**, *30*, e3250. [[CrossRef](#)]
29. Yang, H.; Bergmans, J.; Schenk, T.; Linnartz, J.; Rietman, R. An Analytical Model for the Illuminance Distribution of a Power LED. *Opt. Express* **2008**, *16*, 21641–21646.
30. Ding, J.; Xu, Z.; Hanzo, L. Accuracy of the Point-Source Model of a Multi-LED Array in High-Speed Visible Light Communication Channel Characterization. *IEEE Photonics J.* **2015**, *7*, 14. [[CrossRef](#)]
31. Ghassemlooy, Z.; Popoola, W.; Rajbhandari, S. *Optical Wireless Communications*, 2nd ed.; CRC Press: Boca Raton, FL, USA, 2018; Taylor & Francis Group: Abingdon, UK, 2019. [[CrossRef](#)]
32. Maheepala, M.; Kouzani, A.Z.; Joordens, M.A. Light-Based Indoor Positioning Systems: A Review. *IEEE Sens. J.* **2020**, *20*, 3971–3995. [[CrossRef](#)]
33. Fang, B.T. Trilateration and Extension to Global Positioning System Navigation. *J. Guid. Control Dyn.* **1986**, *9*, 715–717. [[CrossRef](#)]
34. Plets, D.; Almadani, Y.; Bastiaens, S.; Ijaz, M.; Martens, L.; Joseph, W. Efficient 3D Trilateration Algorithm for Visible Light Positioning. *J. Opt.* **2019**, *21*, 05LT01. [[CrossRef](#)]
35. Yang, B.; Guo, L.; Guo, R.; Zhao, M.; Zhao, T. A Novel Trilateration Algorithm for RSSI-Based Indoor Localization. *IEEE Sens. J.* **2020**, *20*, 8164–8172. [[CrossRef](#)]
36. Ruiz, D.; Ureña, J.; García, J.C.; Pérez, C.; Villadangos, J.M.; García, E. Efficient Trilateration Algorithm Using Time Differences of Arrival. *Sens. Actuators A Phys.* **2013**, *193*, 220–232. [[CrossRef](#)]

37. Doukhnitch, E.; Salamah, M.; Ozen, E. An Efficient Approach for Trilateration in 3D Positioning. *Comput. Commun.* **2008**, *31*, 4124–4129. [[CrossRef](#)]
38. Morales-Céspedes, M.; Haas, H.; Armada, A.G. Optimization of the Receiving Orientation Angle for Zero-Forcing Precoding in VLC. *IEEE Commun. Lett.* **2020**, *25*, 921–925.

Disclaimer/Publisher’s Note: The statements, opinions and data contained in all publications are solely those of the individual author(s) and contributor(s) and not of MDPI and/or the editor(s). MDPI and/or the editor(s) disclaim responsibility for any injury to people or property resulting from any ideas, methods, instructions or products referred to in the content.